Preparation of Cellulose/Diatomite Composite Material and its Adsorption Characteristics and Kinetics

Hongfang Zhou,[a] Liang Zhao,[a,*] Runzhou Huang,[a] Yuhang Yang,[a] Zhengle Que,[a] and Yadi Pan [a,b]

The optimal preparation conditions for cellulose/diatomite composite adsorbents (CDAs) were determined to be a diatomite concentration of 40 wt%, a holding temperature of 700 °C, and a holding time of 30 min. Meanwhile, the yield of CDAs was 70.6%, and the methylene blue (MB) adsorption value was 191.8 mg/g. The specific surface area, total pore volume, and average pore size of the CDAs were 489 m^2/g, 0.372 cm^3/g, and 3.04 nm, respectively. It was inferred that the diatomite was cross-linked with the cellulose carbon to form some micropores. Greater MB initial concentrations and pH values improved the adsorption on the CDAs. The MB adsorption behavior of the CDAs was described very well by the pseudo-second-order model. The isotherm models showed relatively high adsorption of MB.

Keywords: Cellulose; Diatomite; Methylene blue; Adsorption characteristics; Kinetics

*Contact information: a: College of Materials Science and Engineering, Nanjing Forestry University, Nanjing 210037, China; b: Co-Innovation Center of Efficient Processing and Utilization of Forest Resources, Nanjing Forestry University, Nanjing 210037, China; *Corresponding author: zl_06@126.com*

INTRODUCTION

The efficient use of biomass resources is an important approach for reducing the overuse of fossil fuels (Huang *et al*. 2019; Liu *et al*. 2019). Biomass provides not only renewable energy but also resources by transforming it into activated carbon, composites, or other adsorbent materials (Huang *et al*. 2020; Xu *et al*. 2020a,b), which can be applied in wastewater treatment (such as in methylene blue (MB) dye wastewater) and other different fields. To solve the problems of environmental pollution and resources, studies on the exploitation and utilization of biomass carbon adsorption materials have become more popular worldwide. Diatomite is one kind of amorphous siliceous mineral that is abundant in many areas of the world. It has high permeability and porosity, small particle size, and high surface area (Song *et al*. 2019), and it can be applied in wastewater treatment (Selvaraj *et al*. 2018). Biomass carbon is easily obtained from many types of biomass at low cost, and the thermal conversion process is environmentally and economically feasible. Therefore, using biomass carbon to support diatomite in environmental applications is beneficial. Previous research has suggested that the adsorption capacity of biomass carbon/diatomite composites is better than that of either pure biomass carbon materials or diatomite (Yu and Fugetsu 2010). Liu *et al*. (2012) reported a heat treatment method (heating temperature: 700 °C; heating time: 3 h, under N_2 atmosphere) for the preparation of porous carbon. In this method, natural diatomite was used as template and catalyst, and the obtained composites showed a hierarchical porous structure, which exhibited better adsorption capacity on MB. Yang *et al*. (2016) found a hypoxic pyrolysis method (heating temperature: 400 °C to 1200 °C; heating time: 4 h) to produce biomass carbon and

diatomite composites. They reported that the MB absorption capacity of the composite (consist of biomass carbon and diatomite) noticeably increased, compared with the single component (biomass carbon or diatomite). However, the heat treatment conditions (such as heating temperature and holding time) and the diatomite concentration affect the adsorption capabilities of the composite adsorbents. Moreover, there have been few studies on the adsorption characteristics and adsorption kinetics of biomass carbon/diatomite composite adsorbents for MB.

Therefore, this study investigated the preparation of biomass (cellulose, one of the largest sources of biomass) carbon and diatomite composite *via* the heat treatment method (different holding temperatures and times). The MB adsorption capacities of the as-prepared samples were determined to identify the optimal preparation condition of the composites. Then, the effects of different MB initial concentrations and different pH values on the adsorption capacity of the optimal composites were examined. To reveal the adsorption mechanism, the adsorption kinetic and isotherm models were analyzed in this study. This research will help reveal the adsorption mechanism and provide some basic data and a theoretical basis for the industrial application of biomass/diatomite composites. It can also inspire new research on biomass carbon composite materials.

EXPERIMENTAL

Materials

Cellulose (microcrystalline, purity ≥ 99.2 wt%, Sinopharm Chemical Reagent Company, Shanghai, China) and diatomite (purity ≥ 85 wt%, Shanghai Fengxian Fengcheng Reagent Factory, Shanghai, China) were selected for this study. According to the reagent information provided by Sinopharm Chemical Reagent Company (Shanghai, China), the chemical structure of cellulose using in this study is shown in Fig. 1. Potassium carbonate (K_2CO_3) (purity ≥ 99.0 wt%, Sinopharm Chemical Reagent Company, Shanghai, China) was used as heat treatment activator for the biomass/diatomite composite material. Methylene blue (Shanghai Macklin Biochemical Company, Shanghai, China) was used to test the adsorption properties of the composite material. Deionized water was supplied by the Nanjing Zhongdong Chemical Reagent Company (Nanjing, China). High purity nitrogen (purity ≥ 99.999 vol%) was purchased from the Nanjing Tianze Gas Company (Nanjing, China) and was applied as the reaction atmosphere of the heat treatment.

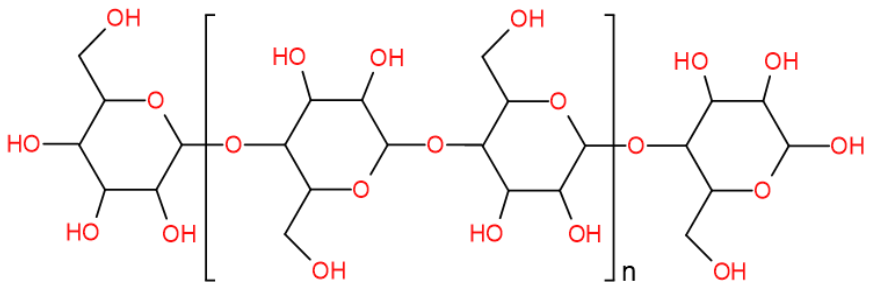

Fig. 1. The chemical structure of raw cellulose in this study (Nehls *et al*. 1994)

Preparation of Composite Adsorbents

Before the heat treatment of the preparation, cellulose and varying concentrations of diatomite (0 wt%, 10 wt%, 20 wt%, 30 wt%, 40 wt%, and 50 wt% in whole mixed materials) were first mixed, and then K_2CO_3 was added into the mixtures (K_2CO_3:cellulose/diatomite = 2:1, by weight). Next, all mixed materials were submerged in 100 mL of deionized water in a glass beaker. Then, these beakers were placed in a 25-°C water bath for 12 h of impregnation (kept still). After the impregnation, the composite materials were immediately dried in an air-dry oven at 105 °C overnight until completely dehydrated.

The preparation of the experimental composite adsorbents was conducted in a ceramic tubular reactor (length 1000 mm, inner diameter 80 mm), which was heated by silicon carbide rods (5 kW). The mixtures were placed in the porcelain boat and then placed into the center part of the tubular furnace. The tubular furnace was continuously injected with high purity nitrogen (N_2 flow rate 200 mL/min). Before heating, the tubular furnace was thoroughly injected with N_2 to remove air. Then, the samples were heated to the holding temperature (400 °C, 500 °C, 600 °C, or 700 °C) at a heating rate of 10 °C/min and a residence time of 30 min, 60 min, 90 min, or 120 min). When the reaction stopped, the cooling down process was developed with the samples inside the oven. After the tubular furnace cooled to room temperature, the composite adsorbents were taken out and washed to neutral with deionized water. The new cellulose/diatomite composite adsorbents were obtained by drying at 105 °C until a constant sample mass was obtained.

Characterization

To determine the phase composition of the composite adsorbent, X-ray diffraction (XRD) measurements were performed using an X-ray diffractometer (Ultima IV, Rigaku Corporation, Tokyo, Japan) equipped with Cu-Kα radiation (40 kV and 40 mA) in the scanning range of 5° to 80° at a scanning rate of 2°/min with a step of 0.02°. To identify functional groups of the composites, Fourier transform infrared (FTIR) spectra were obtained by a FTIR spectrometer (Vertex 80v, Bruker Corporation, Karlsruhe, Germany) within the wavenumber range of 650 cm^{-1} to 4000 cm^{-1}. The microstructure of the composite adsorbent was characterized by scanning electron microscopy (SEM) (Quanta 200, FEI Company, Hillsboro, OR, USA) operated at an acceleration voltage of 15 kV. The Brunauer-Emmett-Teller (BET) surface area and the pore size were measured by N_2 adsorption and desorption (ASAP 2020 HD88, Micromeritics Instrument Corporation, Norcross, GA, USA) at 77 K. An ultraviolet-visible (UV) spectrophotometer (UV1800, Jinghua Science & Technology Instruments Company, Shanghai, China) was used to test the absorbance value of MB at 664 nm.

Adsorption Experiments

To determine the concentrations of the MB solutions, the concentration-absorbance standard curve was obtained by UV spectrophotometry, as shown in Fig. 2. The suspension of adsorbents in the MB solution was shaken in a constant-temperature shaker at a shaking speed of 275 rpm with 25 °C until adsorption equilibrium. The concentration of MB in water was detected by UV spectrophotometry. The adsorption capacity (q_e) of the composite adsorbents for MB was calculated using Eq. 1:

$$q_e = \frac{(C_o - C_e)\,V}{m} \quad (1)$$

where q_e (mg/g) is the equilibrium adsorption capacity, C_o and C_e (mg/L) are respectively the initial and equilibrium MB concentrations, V (L) is the volume of the solution (0.05 L), and m (g) is the mass of the adsorbent (0.005 g).

To reveal the effects of MB initial concentration and pH on the composite adsorption capacity, different mass concentrations of MB (10 mg/L, 15 mg/L, 20 mg/L, 25 mg/L, and 30 mg/L) were prepared. The pH value (3, 5, 7, 9 and 11) of the MB solution (MB initial concentration was 20 mg/L) was adjusted by adding a small amount of 0.1 mol/L HCl or NaOH solution.

The adsorption kinetic and isotherm experiments were performed as described in the literature (Tang *et al*. 2014). The isotherm experimental steps were as follows: preparing the solutions of different MB initial concentrations (10 mg/L, 15 mg/L, 20 mg/L, 25 mg/L, 30 mg/L, and 35 mg/L), the adsorption capacity (q_e) of the composite adsorbents for MB was calculated by Eq. 1. The detailed kinetic experimental steps were as follows: First, 0.005 g of adsorbents and 50 mL of MB solution with an initial concentration of 20 mg/L were placed in a 100-mL glass beaker. Then, the glass beaker was shaken in a mechanical shaker (shaking speed of 275 rpm) at the room temperature (25 °C). At pre-defined time intervals (0.5 h, 1 h, 1.5 h, 2 h, 2.5 h, 3 h, 6 h, and 9 h), 1 mL of the dye solution was taken from the beaker, and the MB concentration was determined. In order to reduce the experimental error, after determining the concentration of MB in each pre-defined time, the solution (tested MB solution of each pre-defined time) was immediately put back into the initial solution. The amount of MB adsorbed per unit mass of adsorbent (q_t, mg/g) at different times (t) was calculated from Eq. 2:

$$q_t = \frac{(C_o - C_t)\,V}{m} \quad (2)$$

where q_t (mg/g) is the MB adsorption capacity at time t, and C_t (mg/L) is the MB concentration at time t.

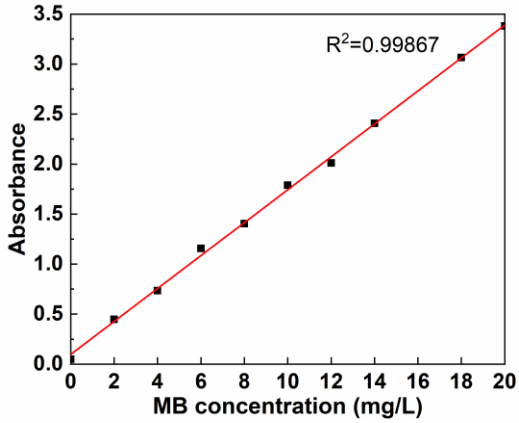

Fig. 2. The concentration-absorbance standard curve of the MB

RESULTS AND DISCUSSION

Influence Factors of Preparation

Effect of diatomite concentration

The solid product yields (on a dry ash-free basis) and MB adsorption values of the composite adsorbents (different diatomite concentrations) are shown in Fig. 3. Figure 3(a)

shows that, with increasing diatomite concentration, the mass yield of the composite adsorbent increased slightly. Yang *et al*. (2016) presented that at 600 °C, the total mass loss of the cellulose decomposition was approximately 70 wt%, while that of the diatomite decomposition was only about 2 wt% (mostly related to the water release and the slight surface changes) *via* the thermogravimetric (TG) analysis, which led to a small increase in the mass yield of the composite adsorbent with the increasing diatomite concentration. The MB adsorption capacity decreased at first, then increased, and then decreasing again (Fig. 3(a)). When 10 wt% to 30 wt% of diatomite was added, the diatomite took the place of part of the cellulose carbon in the whole material, which reduced the MB adsorption capacity. As shown in Fig. 3(b), the calculated theoretical adsorption values (*the adsorption values of biomass carbon* (98.3 mg/g) × *biomass carbon concentration* + *the adsorption values of diatomite* (12.1 mg/g) × *diatomite concentration* (Yang 2019)) for diatomite concentrations of 10 wt% to 30 wt% were greater than the experimental values. Thus, a small amount of diatomite (10 wt% to 30 wt%) had a negative impact on the biomass composite structure. However, as the concentration of diatomite increased to 40 wt% (Fig. 3(a)), the MB adsorption capacity increased. Figure 3(b) shows that the experimental adsorption value at a diatomite concentration of 40 wt% increased to 90.9 mg/g, while the calculated theoretical value was 63.8 mg/g. Therefore, the MB adsorption capacity of the cellulose/diatomite composite adsorbents considerably increased from 30 wt% to 40 wt%. When the addition of diatomite increased to 50 wt%, the MB adsorption capacity dramatically decreased. At that point, excessive diatomite was not conductive to the formation of pores, and the adsorption capacity was greatly reduced. Therefore, the optimal diatomite concentration of the composite adsorbents in this study was approximately 40 wt%.

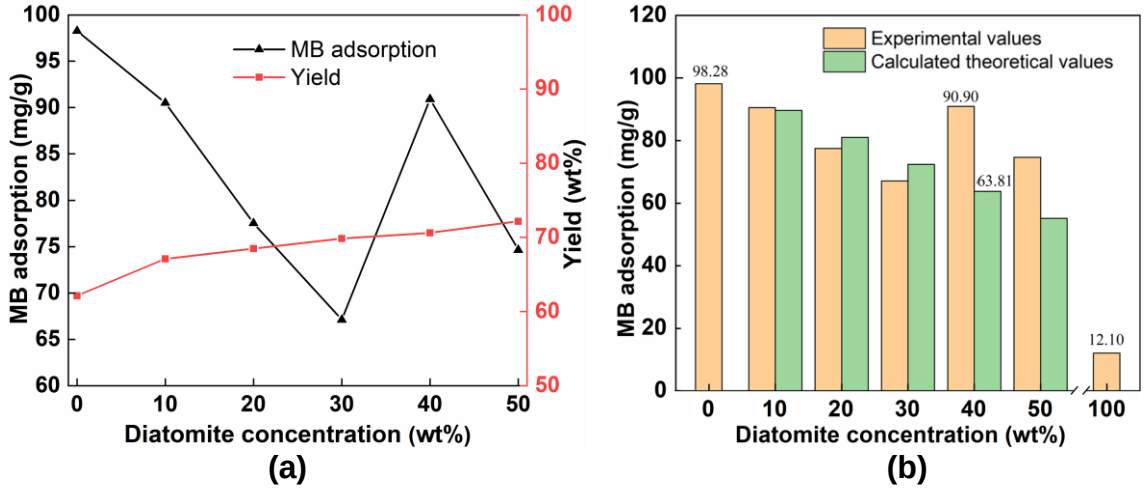

Fig. 3. (a) Mass yields and MB adsorption values ((a) experimental data and (b) experimental and calculated theoretical data) of composite adsorbents with different diatomite concentrations (holding temperature: 600 °C; holding time: 60 min)

Effect of holding temperature

For different holding temperatures (400 °C to 700 °C), the solid product yields and MB adsorption capacities of the composite adsorbents are shown in Fig. 4. As holding temperature increased, the mass yield of the composite adsorbent had a slight decrease, while the MB adsorption value dramatically increased. The TG results of the cellulose decomposition (Yang *et al*. 2016) have shown that the total mass loss of cellulose was more

than 70 wt% from the room temperature to 700 °C. But, in Fig. 4, the total mass loss of the composite adsorbent was unobvious. The reason is that the presence of K_2CO_3 in the interior of the composite inhibited the formation of tar and other liquids (such as acetic acid and methanol) (Guo and Lua 2003). Then the total loss of the cellulose/diatomite decomposition process was only slightly reduced. Besides, because K_2CO_3 can inhibit the shrinkage of the pore in cellulose carbon (Guo and Lua 2003), and K_2CO_3 may react with carbon *via* $K_2CO_3 + 2\ C \rightarrow 2\ K + 3\ CO$, the specific surface area and the pore volume increased with the increases in temperature (Hayashi *et al*. 2002), as shown in Fig. 4. Thus, holding temperature was a key factor affecting the microcrystalline structure and pore structure of the composite adsorbents. As the holding temperature increased, the graphite crystallite structure gradually became orderly, and the degree of graphitization increased (Zhu *et al*. 2014). Specifically, at lower temperatures (< 600 °C), the graphite crystallite and pore structure were not fully developed, resulting in a lower specific surface area and total pore volume (Zhu *et al*. 2014). As the order of the graphite microcrystalline structure increased, and the three-dimensional microcrystalline structure was formed (Zhu *et al*. 2014), the specific surface area and total pore volume of the composite adsorbents were maximized at 700 °C, in this study. However, when the holding temperature further increased (> 700 °C), the graphite crystallite structure should become more ordered; and when the degree of graphitization increased, the pores would be destroyed, and the specific surface area dramatically decreased (Zhu *et al*. 2014). Therefore, the adsorption performance of samples for temperatures greater than 700 °C was not considered in this paper. In general, it can be inferred that the most abundant pores were formed in the three-dimensional microcrystalline structure at 700 °C. Hence, the optimal holding temperature of the composite adsorbents was approximately 700 °C.

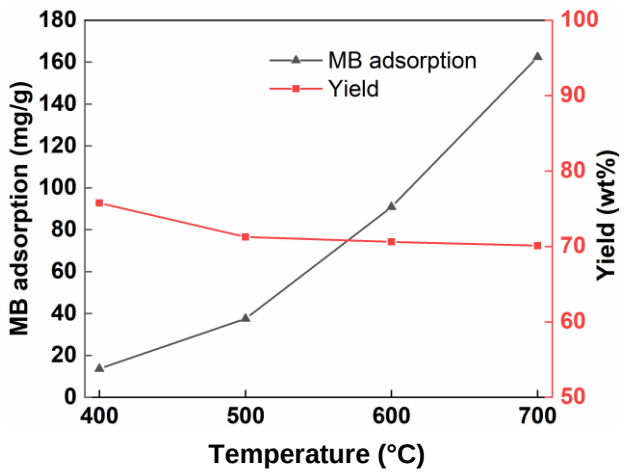

Fig. 4. Mass yields and MB adsorption values of composite adsorbents at different holding temperatures (diatomite concentration: 40 wt%; holding time: 60 min)

Effect of holding time

The effects of holding time on the mass yields and MB adsorption values of the composite adsorbents are shown in Fig. 5. From 30 min to 90 min, the MB adsorption capacity of the composite adsorbents exhibited no obvious changes. This result shows that, with the increase of holding time, the graphite crystallite structure gradually should become more orderly, but the range of change was quite limited. However, when the holding time increased to 120 min, the microcrystalline structure may be destroyed, and some of the

micropores in the adsorbents become mesopores or macropores, thus decreasing specific surface area and pore volume (Zhu *et al*. 2014). To better understand the mechanism here, the thorough BET or microscopy analysis will be carried out in the coming research.

To heat the sample uniformly, the holding time should be set at 30 min to 90 min. Meanwhile, if the holding time is extended to 60 min or 90 min, more energy will be consumed. Therefore, the optimal holding time for the composite adsorbents can be selected as 30 min. Therefore, the overall optimal preparation conditions for the composite adsorbents were a diatomite concentration of 40 wt%, a holding temperature of 700 °C, and a holding time of 30 min. The composite adsorbents prepared under these conditions were named "CDAs" herein. The yield of CDAs was 70.58 %, and the MB adsorption value was 191.76 mg/g.

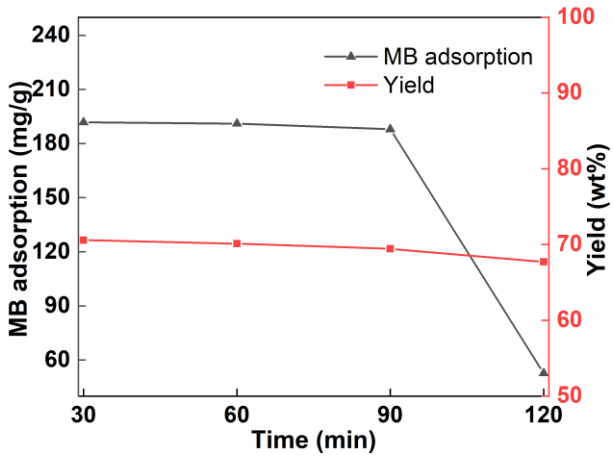

Fig. 5. Mass yields and MB adsorption values of composite adsorbents at different holding times (diatomite concentration: 40 wt%; holding temperature: 700 °C)

Characterization of CDAs

The CDAs were characterized by XRD, FTIR, SEM, and BET analyses, and the results are shown in Fig. 6. In Fig. 6(a), the peak at 26.4° belonged to the typical SiO_2 diffraction peak (Fu *et al*. 2017). Compared to raw diatomite, the diffraction peak at 2θ = 26.4 ° (α-quartz crystal phase) of the CDAs appeared to be weaker. And the characteristic diffraction band of the amorphous protein phase of the CDAs at 2θ = 21.8° and the amorphous diffraction band of the amorphous biochar basically disappeared, indicating that the preparation process had a negative effect on the crystalline phase of the carbon structure, and the quartz phase of diatomite was weakened during the preparation process. Yang (2019) reported that the carbonization of cellulose promoted the crystal quartz into the cristobalite phase. Besides, Sun (2009) pointed out that the diatomite can react with the carbon to form silicon carbide ($SiO_2 + 3\ C \rightarrow SiC + 2\ CO$).

In Fig. 6(b), the wavenumbers of 1560 cm^{-1}, 1375 cm^{-1}, and 996 cm^{-1} were related to the skeletal vibration of the graphitic domains (sp^2 C=C bond), C-O vibration, and Si-O-Si vibration, respectively (Yang *et al*. 2019). Compared to the CDAs, in Fig. 6(b), the C-O vibration (1473 to 1050 cm^{-1}), C-H vibration (2897 cm^{-1}), and O-H vibration (3336 cm^{-1}) of raw cellulose basically disappeared after the carbonization. Accordingly, it can be deduced that carbonization of cellulose led to the decomposition of some groups into volatiles, which was the key to the formation of porous materials. Moreover, the characteristic peak of the amorphous opal structure Si-O-Si bond located at 1063 cm^{-1} and

792 cm^{-1} of raw diatomite were noticeably weakened in CDAs, indicating that the crystal phase of cristobalite was stable in CDAs.

In Fig. 6(c), many micropores surrounded with diatomite are visible. In addition, the morphology of diatomite had been destroyed to varying degrees, indicating that the carbonization of biomass had changed the characteristic morphology of the porous structure of diatomite in CDAs. The curves of N_2 adsorption and desorption are shown in Fig. 6(d). The shape of the N_2 sorption isotherms for the CDAs indicated the presence of micropores and mesopores (Wang and Yuan 2015), which showed good adsorption capacity. From the preliminary BET data, the specific surface area, total pore volume, and average pore size were 488.774 m^2/g, 0.372 cm^3/g, and 3.044 nm, respectively.

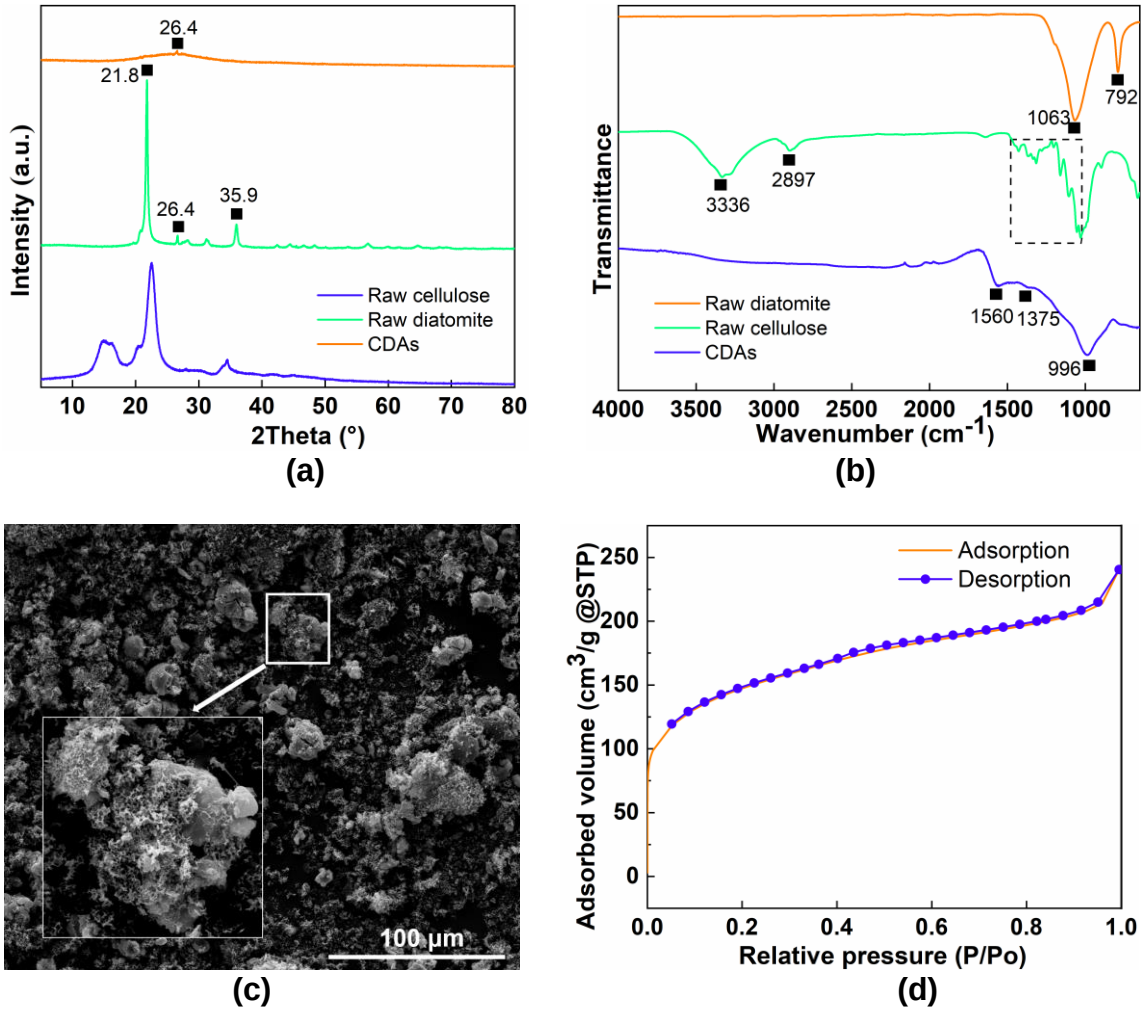

Fig. 6. Characterization of CDAs by (a) XRD, (b) FTIR, (c) SEM, and (d) BET analyses

Effects of MB Solution Environments

The effects of solution environments on the CDAs' adsorption capacity are shown in Fig. 7. As MB initial concentration increased, the MB adsorption capacity of the CDAs gradually increased (Fig. 7(a)). This result indicated that the increase in initial concentration was conducive to competitive adsorption, which increased the adsorption capacity (Zargar *et al*. 2011). Figure 7(b) shows the effect of pH in the range of 3 to 11 (MB initial concentration was 20 mg/L). As pH increased, the MB adsorption values

dramatically increased. At low pH values (pH < 7), H^+ inhibited the MB adsorption capacity. Because MB is a cationic dye, an alkaline environment (decreased H^+ concentration) increases the adsorption (Kong *et al*. 2018).

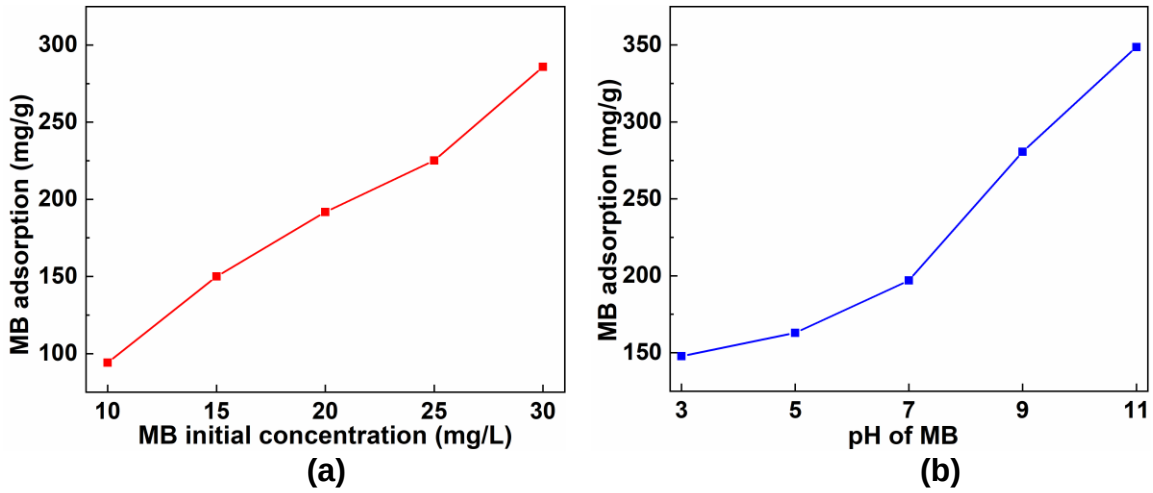

Fig. 7. Effects of (a) MB initial concentration and (b) pH value on MB adsorption capacity of CDAs

Adsorption Kinetics Model Fitting

To understand the dynamic interactions of MB ions with the CDAs and predict the relationship between the adsorption rate and time, the kinetics experimental data were analyzed by the pseudo-first-order and pseudo-second-order models. Based on the previous related studies (Goel *et al*. 2011; Xiao *et al*. 2015), the pseudo-first-order kinetic model (Eq. 3) and pseudo-second-order kinetic model (Eq. 4) can be expressed as follows,

$$\ln(q_e - q_t) = \ln q_e - k_1 t \quad (3)$$

$$\frac{t}{q_t} = \frac{1}{k_2 q_e^2} + \frac{t}{q_e} \quad (4)$$

where q_t and q_e indicate the amount of MB at time t and at equilibrium (mg/g); k_1 and k_2 are the pseudo-first-order rate constant (min^{-1}) and the pseudo-second-order rate constant (g/(mg·min)) for the adsorption process, respectively; and t is the time (min).

The regression plots of the pseudo-first-order kinetic model and pseudo-second-order kinetic model are shown in Figs. 8(a) and 8(b), respectively. The corresponding kinetic parameters for these two kinetic models are shown in Table 1. The pseudo-second-order adsorption kinetic model's R^2 (correlation coefficient) value was greater than that of the pseudo-first-order kinetic model (R^2 = 0.80728). Because the R^2 of the pseudo-second-order model (R^2 = 0.99987) was close to 1, it was inferred that the pseudo-second-order model closely fit the real adsorption process. Moreover, the calculated equilibrium adsorption capacity value ($q_{e,cal}$ = 169 mg/g) with the pseudo-second-order model (Table 1) was close to the experimental equilibrium adsorption capacity value ($q_{e,exp}$ = 192 mg/g). Therefore, the MB adsorption behavior of the CDAs was described well by the pseudo-second-order model. Hubbe *et al*. (2019) discusses about the pseudo-second-order model, and pointed out that the good fits of adsorption data to that model are usually explained by a diffusion-based mechanism.

Table 1. Kinetic Parameters for the Adsorption of MB on CDAs

Kinetic Model	Model Parameters			
Pseudo-first-order kinetic model	k_1 (min^{-1})	$q_{e,cal}$ (mg/g)	$q_{e,exp}$ (mg/g)	R^2
	1.67×10^{-3}	58.62	191.76	0.80728
Pseudo-second-order kinetic model	k_2 (g/(mg·min))	$q_{e,cal}$ (mg/g)	$q_{e,exp}$ (mg/g)	R^2
	3.7247×10^{-4}	168.92	191.76	0.99987

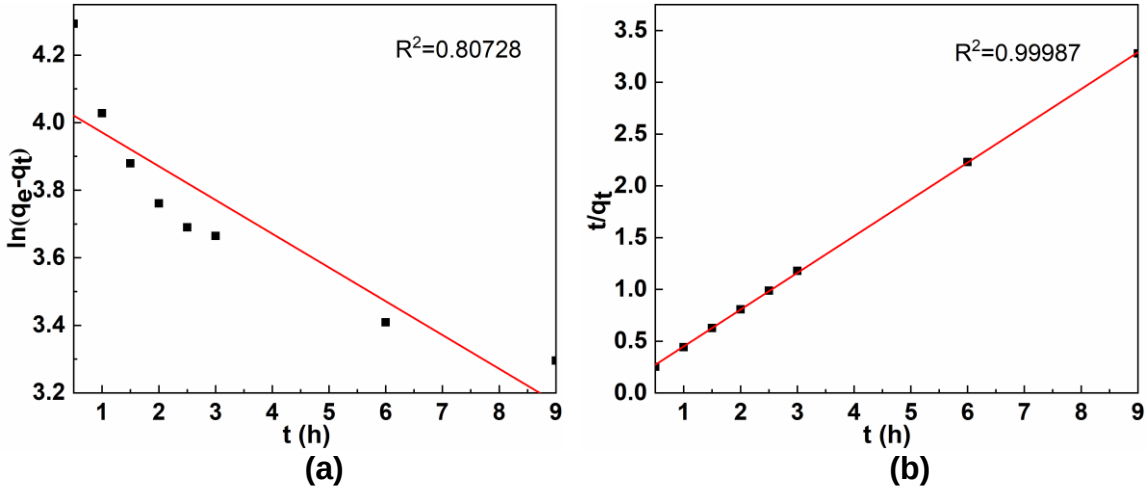

Fig. 8. (a) Pseudo-first-order and (b) pseudo-second-order models for MB adsorption on CDAs

Adsorption Isotherm Model

To determine the surface properties and affinity of the adsorbent and the distribution of the MB ions at equilibrium, equilibrium isotherms were studied. Some typical isotherm models were used to investigate the adsorption mechanism. The Langmuir isotherm equation is suitable for monolayer sorption on the CDA surfaces, which contained a finite number of identical sorption points; the Freundlich equation is an empirical relationship based on sorption on a heterogeneous surface (Caliskan *et al*. 2011). The Langmuir and Freundlich isotherms are not sufficient to clarify the physical and chemical characteristics of adsorption. The Dubinin-Radushkevich (D-R) isotherm is more general than the Langmuir isotherm (Caliskan *et al*. 2011), as it does not assume a homogeneous surface or constant sorption potential. The linearized Langmuir (Eqs. 5 and 6), Freundlich (Eq. 7), and D-R (Eqs. 8 to 10) adsorption equations can be expressed as follows (Caliskan *et al*. 2011; Tang *et al*. 2019; Wei *et al*. 2016):

Langmuir adsorption equation:

$$\frac{C_e}{q_e} = \frac{1}{K_L q_m} + \frac{C_e}{q_m} \quad (5)$$

Another essential feature of the Langmuir isotherm can be expressed in terms of a dimensionless factor (the separation factor, R_L) (Eq. 6):

$$R_L = \frac{1}{1 + K_L C_O} \quad (6)$$

Freundlich adsorption equation:

$$\ln q_e = \ln K_F + \frac{1}{n} \ln C_e \quad (7)$$

D-R adsorption equation:

$$\ln q_e = \ln q_m - \beta\varepsilon^2 \quad (8)$$

$$\varepsilon = R_g T \times \ln(1 + \frac{1}{C_e}) \quad (9)$$

The adsorption energy (E) (kJ/mol) gives information about the adsorption mechanism (chemical ion exchange or physical adsorption) (Caliskan *et al*. 2011) Eq. 10:

$$E = (2\beta)^{-0.5} \quad (10)$$

In Eqs. 5 to 10, q_m (mg/g) is the maximum MB adsorption amount, q_e (mg/g) is the MB adsorption value at equilibrium, K_L (L/mg) and K_F are the Langmuir and Freundlich isotherm constants, n is a heterogeneity factor, β (mol^2/kJ^2) is the heat of adsorption related constant, C_o and C_e are the initial and equilibrium MB concentrations (mg/L), R_g is the gas constant, and T (K) is the MB solution absolute temperature (298 K).

The regression plots of the Langmuir, Freundlich, and D-R isotherm models are shown in Figs. 9(a), 9(b), and 9(c), respectively. The corresponding isotherm parameters for the three isotherm models are shown in Table 2. Ghorai *et al*. (2012) revealed the values of unfavorable adsorption ($R_L > 1$), linear adsorption ($R_L = 1$), irreversible adsorption ($R_L = 0$), and favorable adsorption ($0 < R_L < 1$). The value of R_L was 0.401 (Table 2), which indicated favorable adsorption of MB on the CDAs. The value of n (linear adsorption: $n = 1$; beneficial or favorable adsorption: $1 < n < 10$ (Arfaoui *et al*. 2008)) was 3.594, which also indicated beneficial or favorable adsorption of MB on the CDAs. The best fitting model was the Langmuir ($R^2 = 0.99655$) isotherm model, indicating that the adsorption behavior was predominantly monolayer adsorption, which could be chemical or physical adsorption (Sun *et al*. 2015). In addition, the value of E (adsorption process of chemical ion-exchange: 8 kJ/mol < E < 16 kJ/mol; physical adsorption process: E < 8 kJ/mol (Caliskan *et al*. 2011)) was 1.143 kJ/mol, suggesting the physical adsorption was also included. Overall, based on the results of the adsorption kinetics model and the adsorption isotherm model, it could be concluded that ion-exchange and van der Waals interactions can be responsible for the adsorption process (Mrozik *et al*. 2008). Moreover, because the MB has a positive charge and the adsorbent has a negative charge, it has to be pointed out that the electrostatic forces can be considered as a contribution to the energy of adsorption (Hubbe *et al*. 2019).

Table 2. Isotherm Parameters for the Adsorption of MB on CDAs

Isotherm Model	Model Parameters		
Langmuir isotherm model	q_m (mg/g)	R_L	R^2
	200.40	0.401	0.99655
Freundlich isotherm model	n		R^2
	3.594		0.95017
D-R isotherm model	q_m (mg/g)	E (kJ/mol)	R^2
	156.97	1.143	0.80567

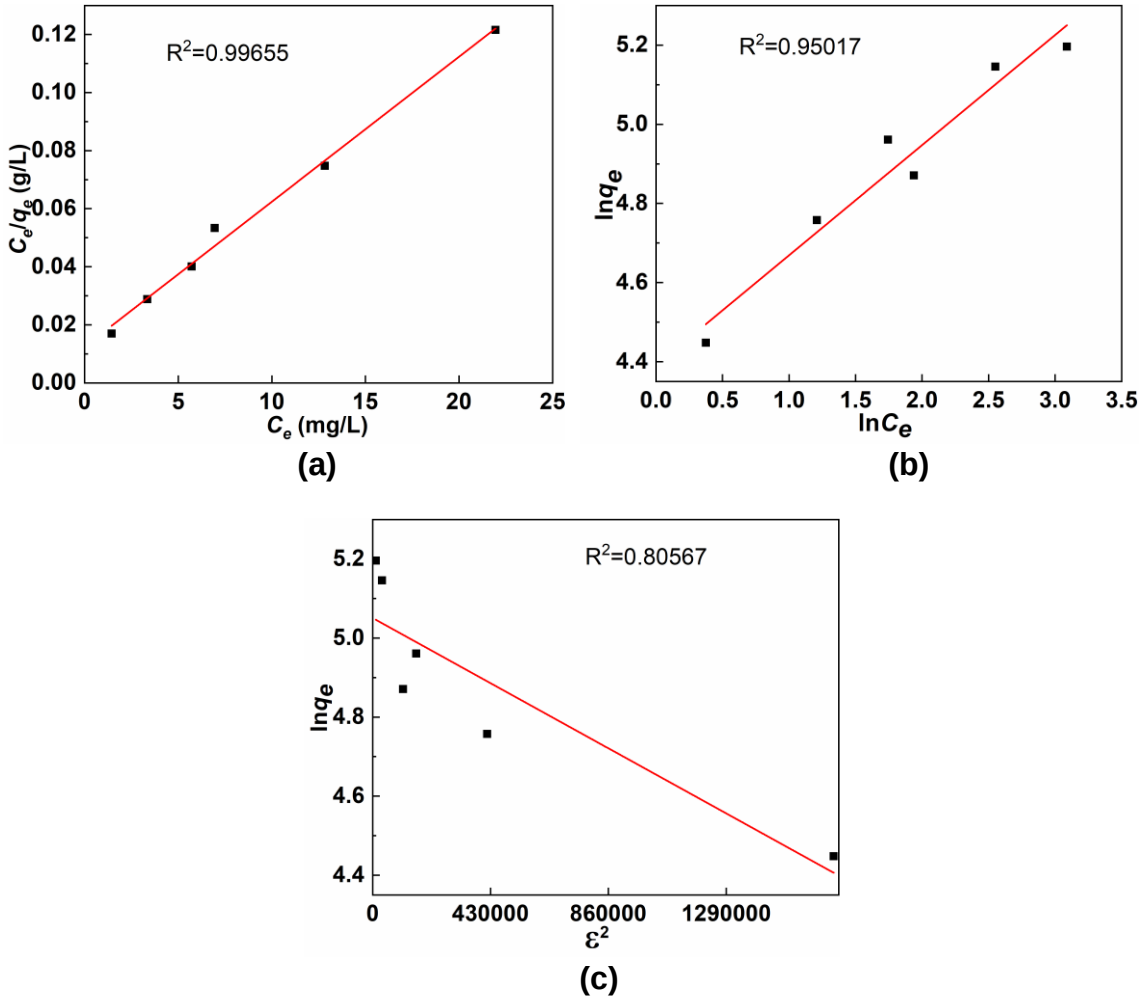

Fig. 9. (a) Langmuir, (b) Freundlich, and (c) D-R isotherm models for MB adsorption on CDAs

CONCLUSIONS

1. The optimal preparation conditions for the cellulose/diatomite composite adsorbents were a diatomite concentration of 40 wt%, a holding temperature of 700 °C, and a holding time of 30 min. The yield was 70.6%, and the methylene blue (MB) adsorption value was 192 mg/g. A diatomite concentration of 40 wt% achieved the optimal balance of biomass carbon structure. Holding temperature was a key factor affecting the adsorption capacity composite adsorbents.
2. Based on X-ray diffraction (XRD) and Fourier transform infrared (FTIR) analyses, it can be inferred that cellulose carbon promoted the crystallization and crystal transformation process of siliceous components in diatomite, and also changed the functional group distribution on the surface of cellulose-diatomite composite adsorbents (CDAs). Scanning electron microscopy showed many micropores surrounded with diatomite. The preliminary BET analysis of the CDAs indicated the existence of micropores and mesopores. The specific surface area, total pore volume, and average pore size were 489 m^2/g, 0.372 cm^3/g, and 3.04 nm, respectively.

3. With the increase of MB initial concentration, the MB adsorption capacity of the CDAs gradually increased. This result indicated that the increase in initial concentration was conducive to competitive adsorption. Meanwhile, a more alkaline solution environment improved the adsorption, because H^+ would inhibit the MB adsorption capacity. The electrostatic forces play a role in the adsorption.
4. The MB adsorption behavior of the CDAs was described very well by the pseudo-second-order model. The Langmuir and Freundlich isotherm models showed good adsorption of MB on the CDAs. The value of R_L was 0.401, which indicated favorable adsorption. The value of n was 3.594, which also indicated good adsorption. In the D-R isotherm model, the value of E was 1.143 kJ/mol, suggesting that the physical adsorption was also included in the adsorption process. It could be concluded that ion-exchange and van der Waals interactions were responsible for the adsorption process.

ACKNOWLEDGMENTS

The research was financially supported by the Natural Science Foundation of Jiangsu, China (18KJA220002), the Opening Research Fund Program of the Key Laboratory of Energy Thermal Conversion and Control of Ministry of Education of Southeast University (No. 2016007), and the Practice Innovation Training Program for College Students in Jiangsu Province (201910298003Y). The authors acknowledge the support of the Advanced Analysis and Testing Center of Nanjing Forestry University.

REFERENCES CITED

Arfaoui, S., Frini-Srasra, N., and Srasra, E. (2008). "Modelling of the adsorption of the chromium ion by modified clays," *Desalination* 222(1-3), 474-481. DOI: 10.1016/j.desal.2007.03.014

Caliskan, N., Kul, A. R., Alkan, S., Sogut, E. G., and Alacabey, I. (2011). "Adsorption of zinc(II) on diatomite and manganese-oxide-modified diatomite: A kinetic and equilibrium study," *Journal of Hazardous Materials* 193, 27-36. DOI: 10.1016/j.jhazmat.2011.06.058

Fu, Y., Xu, X., Huang, Y., Hu, J., Chen, Q., and Wu, Y. (2017). "Preparation of new diatomite–chitosan composite materials and their adsorption properties and mechanism of Hg(II)," *Royal Society Open Science* 4(12). DOI: 10.1098/rsos.170829

Ghorai, S., Sinhamahpatra, A., Sarkar, A., Panda, A. B., and Pal, S. (2012). "Novel biodegradable nanocomposite based on XG-g-PAM/SiO_2: Application of an efficient adsorbent for Pb^{2+} ions from aqueous solution," *Bioresource Technology* 119, 181-190. DOI: 10.1016/j.biortech.2012.05.063

Goel, N. K., Kumar, V., Pahan, S., Bhardwaj, Y. K., and Sabharwal, S. (2011). "Development of adsorbent from Teflon waste by radiation induced grafting: Equilibrium and kinetic adsorption of dyes," *Journal of Hazardous Materials* 193, 17-26. DOI: 10.1016/j.jhazmat.2011.05.026

Guo, J., and Lua, A. C. (2003). "Textural and chemical properties of adsorbent prepared from palm shell by phosphoric acid activation," *Materials Chemistry and Physics* 80(1), 114-119. DOI: 10.1016/S0254-0584(02)00383-8

Hayashi, J., Horikawa, T., Takeda, I., Muroyama, K., and Ani, F. N. (2002). "Preparing activated carbon from various nutshells by chemical activation with K_2CO_3," *Carbon* 40(13), 2381-2386. DOI: 10.1016/S0008-6223(02)00118-5

Huang, Y., Gao, Y. X., Zhou, H., Sun, H. Q., Zhou, J. B., and Zhang, S. (2019). "Pyrolysis of palm kernel shell with internal recycling of heavy oil," *Bioresource Technology* 272, 77-82. DOI: 10.1016/j.biortech.2018.10.006

Huang, Y., Liu, S. S., Zhang, J., Syed-Hassan, S. S. A., Hu, X., Sun, H. Q., Zhu, X., Zhou, J. B., Zhang, S., and Zhang, H. (2020). "Volatile–char interactions during biomass pyrolysis: Cleavage of C–C bond in a β–5 lignin model dimer by amino-modified graphitized carbon nanotube," *Bioresource Technology* 307, Article number 123192. DOI: 10.1016/j.biortech.2020.123192

Hubbe, M. A., Azizian, S., and Douven, S. (2019). "Implications of apparent pseudo-second-order adsorption kinetics onto cellulosic materials: A review," *BioResources* 14(3), 7582-7626. DOI: 10.15376/biores.14.3.7582-7626

Kong, Y., Zhuang, Y., Shi, B. Y., Han, Z. Y., Hao, H. T., Han, K., and Yu, J. W. (2018). "Adsorption of methylene blue and Cu(II) by activated carbon / macromolecule composite hydrogel," *Environmental Science* 39(2), 819-827. DOI: 10.13227/j.hjkx.201707041

Liu, D., Yuan, P., Tan, D. Y., Liu, H. M., Wang, D., Fan, M. D., Zhu, J. X., and He, H. P. (2012). "Facile preparation of hierarchically porous carbon using diatomite as both template and catalyst and methylene blue adsorption of carbon products," *Journal of Colloid and Interface Science* 388, 176-184. DOI: 10.1016/j.jcis.2012.08.023

Liu, S., Wu, Y., Zhang, J., Gao, W., Zhou, J. B., Huang, Y., Zhang, S., and Zhang, H. (2019). "Volatile–char interactions during biomass pyrolysis: A Case study of a lignin model compound and functionalized graphitized carbon nanotubes," *Energy Fuels* 33(11), 11339-11345. DOI: 10.1021/acs.energyfuels.9b03247

Mrozik, W., Jungnickel, C., Skup, M., Urbaszek, P., and Stepnowski, P. (2008). "Determination of the adsorption mechanism of imidazolium-type ionic liquids onto kaolinite: Implications for their fate and transport in the soil environment," *Environmental Chemistry* 5(4), 299-306. DOI: 10.1071/EN08015

Nehls, I., Wagenknecht, W., Philipp, B., and Stscherbina, D. (1994). "Characterization of cellulose and cellulose derivatives in solution by high resolution ^{13}C-NMR spectroscopy," *Progress in Polymer Science* 19(1), 29-78. DOI: 10.1016/0079-6700(94)90037-X

Selvaraj, K., Sidek, L. M., Noor, M. J. M. M., Tamunaidu, P., and Goto, M. (2018). "Alternative approach to conventional river water treatment using natural coagulant," *International Journal of Engineering and Technology* 7(4), 739-742. DOI: 10.14419/ijet.v7i4.35.23099

Song, Y., Yuan, P., Wei, Y., Liu, D., Tian, Q., Zhou, J., Du, P., Deng, L., Chen, F., and Wu, H. (2019). "Constructing hierarchically porous nestlike Al_2O_3–MnO_2@diatomite composite with high specific surface area for efficient phosphate removal," *Industrial & Engineering Chemistry Research* 58(51), 23166-23174. DOI: 10.1021/acs.iecr.9b05574

Sun, Y. (2009). *Structural Transition of Silicon Dioxide, Carbon and Silicon under High Pressure and High Temperature.* Master's Thesis, Jilin University, Changchun, China

Sun, L., Chen, D. M., Wan, S. G., and Yu, Z. B. (2015). "Performance, kinetics, and equilibrium of methylene blue adsorption on biochar derived from eucalyptus saw dust modified with citric, tartaric, and acetic acids," *Bioresource Technology* 198,

300-308. DOI: 10.1016/j.biortech.2015.09.026

Tang, Y., Hu, T., Zeng, Y., Zhou, Q., and Peng, Y. (2014). "Effective adsorption of cationic dyes by lignin sulfonate polymer based on simple emulsion polymerization: isotherm and kinetic studies," *RSC Advances* 5(5), 3757-3766. DOI: 10.1039/C4RA12229A

Tang, Y., Zhao, Y., Lin, T., Li, Y., Zhou, R., and Peng, Y. (2019). "Adsorption performance and mechanism of methylene blue by H_3PO_4-modified corn stalks," *Journal of Environmental Chemical Engineering* 7(6). DOI: 10.1016/j.jece.2019.103398

Wang, W., and Yuan, D. (2015). "Mesoporous carbon originated from non-permanent porous MOFs for gas storage and CO_2/CH_4 separation," *Scientific Reports* 4. DOI: 10.1038/srep05711

Wei, W., Wang, Q., Li, A., Yang, J., Ma, F., Pi, S., and Wu, D. (2016). "Biosorption of Pb (II) from aqueous solution by extracellular polymeric substances extracted from Klebsiella sp. J1: Adsorption behavior and mechanism assessment," *Scientific Reports* 6(1). DOI: 10.1038/srep31575

Xiao, L., Xiong, Y., Tian, S., He, C., Su, Q, and Wen, Z. (2015). "One-dimensional coordination supramolecular polymer $[Cu(bipy)(SO4)]_n$ as an adsorbent for adsorption and kinetic separation of anionic dyes," *Chemical Engineering Journal* 265, 157-163. DOI: 10.1016/j.cej.2014.11.134

Xu, L., Li, Y., Gao, S. Y., Niu, Y., Liu, H. X., Mei, C. T., Cai, J. B., and Xu, C. Y. (2020a). "Preparation and properties of cyanobacteria-based carbon quantum dots/polyvinyl alcohol/ nanocellulose composite," *Polymers* 12(5), Article number 1143. DOI: 10.3390/polym12051143

Xu, L., Zhang, Y. S., Pan, H. Q., Xu, N., Mei, C. T., Mao, H. Y., Zhang, W. Q., Cai, J. B., and Xu, C. Y. (2020b). "Preparation and performance of radiata-pine-derived polyvinyl alcohol/carbon quantum dots fluorescent films," *Materials* 13(1), Article number 67. DOI: 10.3390/ma13010067

Yang, X., Jiang, Y., Su, R., Yang, G., Xue, B., and Li, F. (2016). "Effects of cellulose carbonization on biomass carbon and diatomite composite," *Colloids and Surfaces A: Physicochemical and Engineering Aspects* 509, 314-322. DOI: 10.1016/j.colsurfa.2016.09.021

Yang, X., Jiang, Y., Xue, B., Xia, M., Luo, F., Xu, S., and Li, F. (2019). "Microstructure and properties of *in-situ* prepared cellulosic biomass carbon based diatomite composite," *Materials Science and Technology* 35(4), 469-476. DOI: 10.1080/02670836.2019.1570660

Yang, X. D. (2019). *Surface Effects of Biomass Carbonization and Diatomite/Montmorillonite*, Ph.D. Dissertation, Jilin University, Changchun, China

Yu, H., and Fugetsu, B. (2010). "A novel adsorbent obtained by inserting carbon nanotubes into cavities of diatomite and applications for organic dye elimination from contaminated water," *Journal of Hazardous Materials* 177(1-3), 138-145. DOI: 10.1016/j.jhazmat.2009.12.007

Zargar, B., Parham, H., and Rezazade, M. (2011). "Fast removal and recovery of methylene blue by activated carbon modified with magnetic iron oxide nanoparticles," *Journal of the Chinese Chemical Society* 58(5), 694-699. DOI: 10.1002/jccs.201190108

Zhu, Q. Q., Zhou, H. L., Li, W. J., Chang, Z. D., and Sun, C. Y. (2014). "Structural evolution of cellulose during carbonization and activation," *Journal of University of Science and Technology Beijing* 36(11), 1545-1551. DOI: 10.13374/j.issn1001-053x.2014.11.018

Article submitted: August 10, 2020; Peer review completed: September 12, 2020; Revised version received and accepted: September 21, 2020; Published: September 25, 2020.
DOI: 10.15376/biores.15.4.8728-8743